Available online at www.sciencedirect.com
ScienceDirect
Trans. Nonferrous Met. Soc. China 28(2018) 36−46
Transactions of Nonferrous Metals Society of China
www.tnmsc.cn

Influence of heat treatments on microstructure and mechanical properties of laser additive manufacturing Ti−5Al−2Sn−2Zr−4Mo−4Cr titanium alloy

Yan-yan ZHU, Bo CHEN, Hai-bo TANG, Xu CHENG, Hua-ming WANG, Jia LI

National Engineering Laboratory of Additive Manufacturing for Large Metallic Components,
School of Materials Science and Engineering, Beihang University, Beijing 100083, China

Received 4 August 2016; accepted 21 June 2017

Abstract: The effect of heat treatments on laser additive manufacturing (LAM) Ti−5Al−2Sn−2Zr−4Mo−4Cr titanium alloy (TC17) was studied aiming to optimize its microstructure and mechanical properties. The as-deposited sample exhibits features of a mixed prior β grain structure consisting of equiaxed and columnar grains, intragranular ultra-fine α laths and numerous continuous grain boundary α (α_{GB}). After being pre-annealed in $\alpha+\beta$ region (840 °C) and standard solution and aging treated, the continuous α_{GB} becomes coarser and the precipitate free zone (PFZ) nearby the α_{GB} transforms into a zone filled with ultra-fine secondary α (α_S) but no primary α (α_P). When pre-annealed in single β region (910 °C), all α phases transform into β phase and the alloying elements distribute uniformly near the grain boundary. Discontinuous α_{GB} and uniform mixture of α_P and α_S near grain boundary form after subsequent solution and aging treatment. The two heat treatments can improve the tensile mechanical properties of LAM TC17 to satisfy the aviation standard for TC17.

Key words: laser additive manufacturing; TC17 titanium alloy; heat treatment; microstructure; mechanical properties

1 Introduction

Titanium alloys are widely used in aerospace industries due to their high specific strength, good room and high temperature mechanical properties and excellent corrosion resistance [1−3]. Ti−5Al−2Sn−2Zr−4Mo−4Cr (named TC17 in China and Ti-17 in America) is a near β titanium alloy mainly used to fabricate the compressor disk, blade or integrated blisk components of advanced aircraft engines at temperatures up to 450 °C [4,5]. Manufacturing these large and key load-bearing titanium alloy components by traditional wrought-based processes usually results in time-consuming, low materials utilization ratio and high buy-to-fly ratio. These shortcomings could be obviously overcome by the rapidly developing laser additive manufacturing (LAM) technique, a rapid solidification process based on layer-by-layer materials melting and depositing to fabricate fully dense near-net-shape metallic components [6−10].

Due to the near-net shape nature of LAM process, the LAM components cannot be post-deformed and the heat treatment is one of the most important approaches to optimize the microstructure and mechanical properties of LAM titanium alloys. Traditional solution treatment, namely pre-treatment and solution treatment in $\alpha+\beta$ region followed by aging, has been proved to be optimum heat treatment for the conventional wrought near β titanium alloys [11,12]. However, the as-deposited LAM near β titanium alloys are commonly characterized by large prior β grains including columnar and equiaxed grains, intragranular ultrafine basket-weave microstructure and numerous continuous grain boundary α (α_{GB}), which are obviously different from the conventional wrought parts [13−15]. Due to these features, the LAM near β titanium alloys often show higher strength and disastrous lower ductility in comparison to the corresponding wrought parts and cannot meet the requirements for engineering applications [13,14,16].

Because the microstructures of LAM titanium alloys are quite different from the wrought parts, the effect of traditional solution treatments might also be completely different from those on wrought parts [17,18].

Foundation item: Project (BX201600010) supported by the National Postdoctoral Program for Innovative Talents of China; Project (2015QNRC001) supported by the Young Elite Scientist Sponsorship Program of China
Corresponding author: Jia LI; Tel/Fax: +86-10-82339691; E-mail: lijia@buaa.edu.cn
DOI: 10.1016/S1003-6326(18)64636-9

Therefore, studying the method to optimize the microstructure and obtain better mechanical properties by heat treatments is very significant for LAM near β titanium alloys. However, very little work has been done until now since most studies related to the LAM titanium alloys were focused on the $\alpha+\beta$ titanium alloys especially for the Ti−6Al−4V [7,9,19−22]. LIU et al [16,23] found that the continuous α_{GB} with the accompanying precipitate free zone (PFZ) is the main reason for the low ductility of LAM TC18 since the crack prefers to nucleating and propagating along the α_{GB}, resulting in intergranular fracture. And they found that the subtransus triplex heat treatment had better effect on the breakage of continuous α_{GB} and the improvement of ductility compared to the standard treatment despite of its narrow temperature window. In addition, according to the knowledge of the wrought titanium alloys, heat treatment in the single β region even for short time will inevitably lead to noticeable increasing of prior β grains and decreasing of mechanical properties [12,24]. However, it was reported that, unlike the $\alpha+\beta$ titanium alloys, the LAM near β titanium alloy showed no obvious grain growth behavior during heating in the single β region (about 15 °C above the β transus temperature) even for 0.5 h, possibly due to its good high temperature stability or original large prior β grains [25,26]. This result indicated an alternative heat treatment for the LAM near β titanium alloys to change the microstructures and mechanical properties.

In this study, the LAM TC17 titanium alloys were annealed in standard $\alpha+\beta$ region and single β phase region and further solution and aging treated in an attempt to investigate the effect of annealing temperature on the microstructure evolution and tensile mechanical properties. The attention was paid to the changing of the continuous α_{GB} and the PFZ and the effect on the tensile properties.

2 Experimental

A thick plate of TC17 alloy with a geometrical size of 300 mm × 200 mm × 35 mm was fabricated by laser additive manufacturing process using a 8 kW laser additive manufacturing system in an argon purged processing chamber with an oxygen content less than 60×10^{-6}. Spherical powders with a particle size ranging from 45 to 212 μm were used as the raw materials, which were produced by plasma atomization process. The laser deposition processing parameters were listed as follows: laser nominal output power 6 kW, laser beam diameter 6−7 mm, beam travel speed 1000 mm/min, powder feed rate 800−1000 g/h. The β transus temperature (T_β) of the as-deposited TC17 sample was (895±5) °C, determined by metallographic method.

12 specimens with a geometric size of 25 mm × 25 mm × 20 mm were machined by electric discharge wire cutting from the plate-like sample, and numbered from 1 to 12, respectively. Firstly, as shown in Table 1, Samples 1−6 and 7−12 were annealed at 840 and 910 °C for 1 h followed by air cooling, respectively. Then, Samples 2−6 and 8−12 were further solution-treated by holding for 0.5, 1, 2 and 4 h at 800 °C, respectively. Finally, on the basis of annealing and solution, Samples 6 and 12 were aged at 630 °C for 8 h. Longitudinal metallographic specimens were prepared by standard mechanical polishing and etched in a mixture solution of HF: HNO_3: H_2O with a volume ratio of 1: 6: 43. An OLYMPUS BX51M optical microscope (OM) and a Camscan 3400 scanning electron microscope (SEM) were used to observe the microstructure and fractography.

Table 1 Heat treatment details for LAM TC17 alloys

Sample No.	Heat treatment		
	Annealing	Solution	Aging
1	(840 °C, 1 h)+AC	−	−
2	(840 °C, 1 h)+AC	(800 °C, 0.5 h)+WQ	−
3	(840 °C, 1 h)+AC	(800 °C, 1 h)+WQ	−
4	(840 °C, 1 h)+AC	(800 °C, 2 h)+WQ	−
5	(840 °C, 1 h)+AC	(800 °C, 4 h)+WQ	−
6	(840 °C, 1 h)+AC	(800 °C, 4 h)+WQ	(630 °C, 8 h)+AC
7	(910 °C, 1 h)+AC	−	−
8	(910 °C, 1 h)+AC	(800 °C, 0.5 h)+WQ	−
9	(910 °C, 1 h)+AC	(800 °C, 1 h)+WQ	−
10	(910 °C, 1 h)+AC	(800 °C, 2 h)+WQ	−
11	(910 °C, 1 h)+AC	(800 °C, 4 h)+WQ	−
12	(910 °C, 1 h)+AC	(800 °C, 4 h)+WQ	(630 °C, 8 h)+AC

Room temperature tensile properties were tested according to the testing standard of ISO 6892−1:2009 at the National Analysis Center for Iron & Steel of China. The tensile specimen was dog-bone with a gauge diameter of 5 mm and a gauge length of 25 mm. All specimens were along deposition direction and located in the middle of the LAM plate-like sample. Three samples of each condition were tested for an average to reduce the measuring error.

3 Results

3.1 Microstructures

3.1.1 As-deposited alloy

The microstructures of as-deposited LAM TC17 alloy are shown in Fig. 1. According to the layer bands features, the contour of the melting pool can be distinguished. The prior β grains (Fig. 1(a)) consist of huge columnar grains, small columnar grains and small equiaxed grains. Small equiaxed grains and small columnar grains are placed alternately in the center zone of each melting pool, while the huge columnar grains are placed in the overlap zone. Both huge columnar grains and small ones are basically parallel to the deposition direction due to the large temperature gradient towards the substrate during the LAM process. The thickness of each deposited layer and the height of small columnar grains depend on the detailed LAM processing parameters. The formation mechanism of the special mixture of columnar grains and equiaxed grains has been clearly explained in the authors' previous work [25,27], here no longer expatiation is given. It should be noted that the TC17 alloy has higher alloying degree than the TC11 alloy, thus under the same LAM parameters, the volume fraction of the equiaxed grains in LAM TC17 alloy is higher than that in LAM TC11 sample according to the solidification principle.

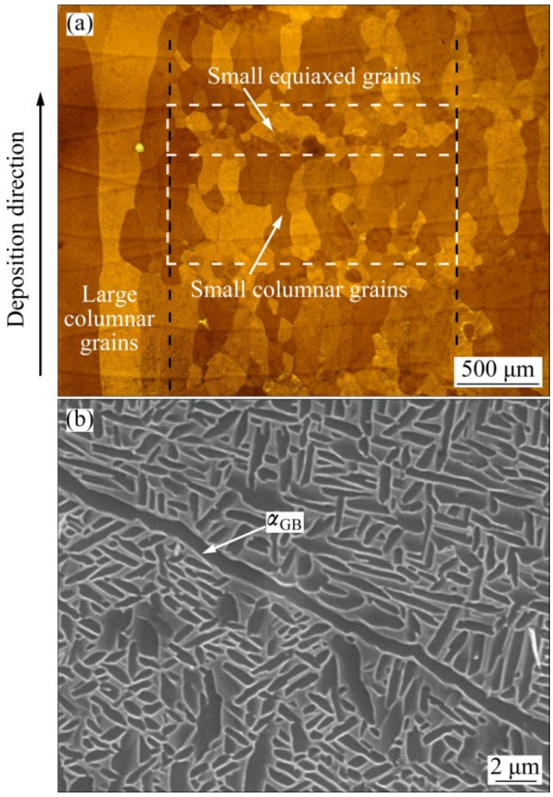

Fig. 1 OM (a) and SEM (b) images showing microstructure of as-deposited LAM TC17 alloy

An ultra-fine basket-weave microstructure resulting from the rapid solidification rate can be observed in most representative regions, as shown in Fig. 1(b). The width of α lath is approximately 0.5 μm, and its length is 1−4 μm. The continuous grain boundary α (α_{GB}) is about 0.7 μm in width, which is much wider than that of the intragranular α lath.

3.1.2 Microstructures after pre-annealed treatment

After being annealed at 840 °C (T_β−45 °C, Fig. 2(a)), some α phases dissolve with the volume fraction of α_P reducing from 70% to 45% compared with the as-deposited sample (Fig. 1(b)). Besides, the width of α lamella decreases to about 0.3 μm with length of 1−2 μm. It is noted that many continuous α_{GB} phases with width of about 0.8 μm still exist. Moreover, an apparent α precipitation free zone (PFZ) with 1.5 μm in width appears on each side of the continuous α_{GB}. The PFZ is a common phenomenon in near β titanium alloys. The above results indicate that when annealing at 840 °C the α phases nearby the α_{GB} prefer to transforming into β prior to other intragranular α lamella and the α_{GB} even coarsens a little instead of dissolving. This transformation is similar to the Ostwald ripening process. When the as-deposited sample is heated in single β region for 1 h (Fig. 2(b)), both the intragranular lamellar α and the α_{GB} dissolve to form single β phase. During the subsequent air cooling stage, no obvious α phase precipitates from the β matrix due to the rapid cooling rate and the high content of β stability elements in TC17 alloy.

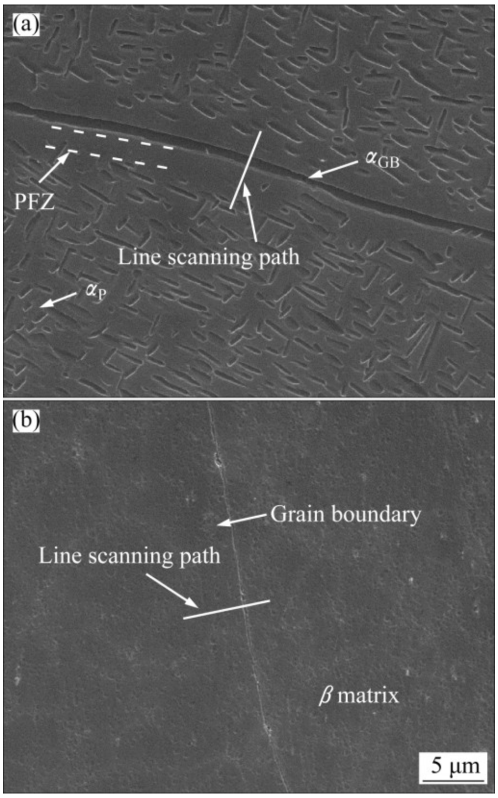

Fig. 2 Microstructures of Sample 1 ((840 °C, 1 h)+AC) (a) and Sample 7 ((910 °C, 1 h)+AC) (b)

Figure 3 shows the constituent fluctuation measured by line scanning across grain boundary of Samples 1 and

7. Both of them were tested by energy spectrometer for about 200 s. The scanning paths were signed as white solid line in Fig. 2 and the signal intensity of each element was revealed in Fig. 3. In Sample 1 annealed at 840 °C, the α_{GB} was continuous and contained higher content of aluminum (Al) and lower contents of molybdenum (Mo) and chromium (Cr), which were opposite to those of PFZ (Fig. 3(a)). For Sample 7, annealing-treatment above T_β made all α phases transform into β phase, α_{GB} and α_P disappeared and all the elements distributed more homogeneously near the grain boundary (Fig. 3(b)).

3.1.3 Microstructures after solution treatment

Figure 4 shows the microstructures of Samples 2−5 which were solution treated at 800 °C for different time. At the beginning of solution, a few α phase precipitates adhered to the α_P and α_{GB}, and soon the volume fraction of α would come up to an equilibrium state, as the solution temperature was 40 °C lower than annealing temperature. In the following solution treatment, α_P and α_{GB} became coarsened, the quantity and the aspect ratio of α_P reduced with the extension of time, while the width of PFZ and continuous α_{GB} did not significantly change.

For the β-annealed alloy, α phase has transformed into β phase completely. After being heated at 800 °C for 0.5 h, as illustrated in Fig. 5(a), the α_{GB} prefers to precipitating at different sites along the grain boundary due to its higher energy state than the intragranular

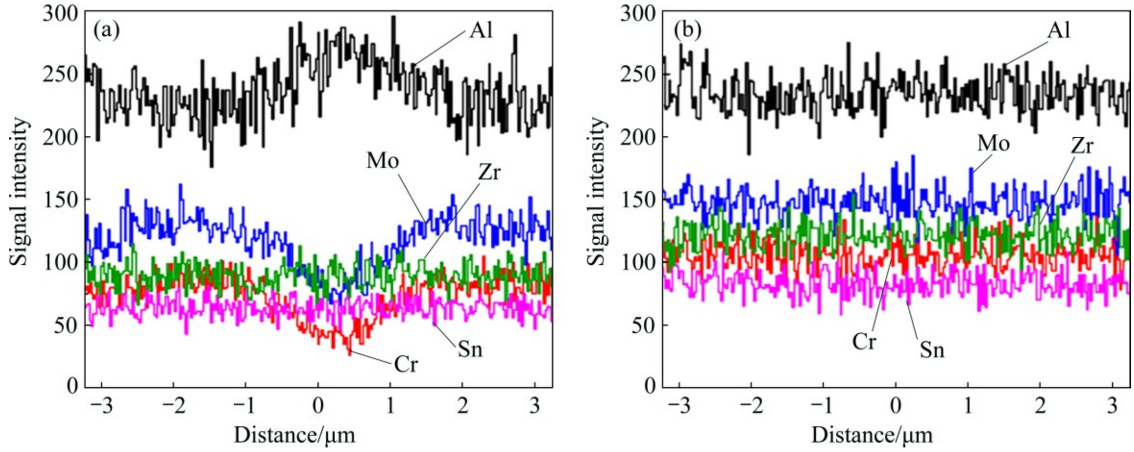

Fig. 3 Constituent fluctuation measured by line scanning across grain boundary in samples annealed at 840 °C (a) and 910 °C (b)

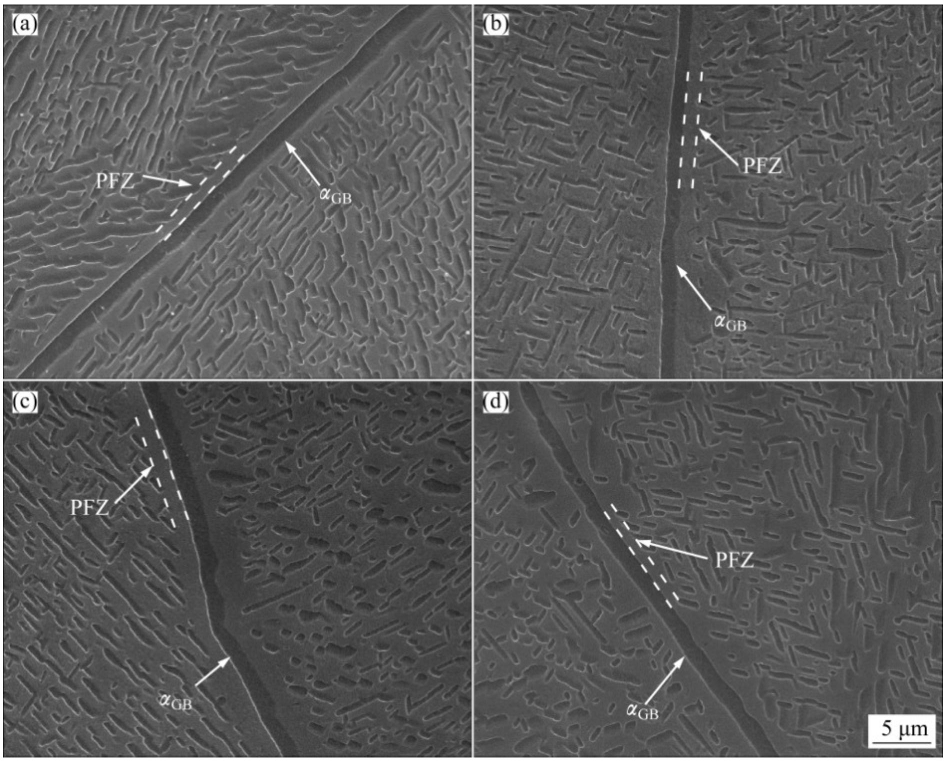

Fig. 4 Microstructures of Samples 2−5 solution treated at 800 °C for different time after 840 °C pre-annealing: (a) Sample 2, 0.5 h; (b) Sample 3, 1 h; (c) Sample 4, 2 h; (d) Sample 5, 4 h

matrix. Then, high aspect ratio but discontinuous α_{GB} forms. Subsequently, large amounts of ultra-fine α_P phases with high aspect ratio precipitate from the β matrix. Because α phase could homogeneously nucleate from single β phase matrix at grain boundary and interior, the PFZ would not form. With prolonging the holding time at 800 °C, α_P and α_{GB} grow up and coarsen gradually. After the volume fraction of α phase increases up to a near equilibrium level, the coarsening process continues. It is worthwhile to note that the α_{GB} exhibits a more obvious coarsening and spheroidizing effect compared to intragranular α phase. In the 2 h and 4 h samples (Figs. 5(c) and (d)), most of the α_{GB} becomes isolate and equiaxed. Compared with the $\alpha+\beta$ annealed samples (Fig. 4), the most significant differences are that the α_{GB} is more discontinuous and equiaxed and no obvious PFZ exists besides the α_{GB} or the grain boundary in the β annealed samples (shown in Figs. 4 and 5).

3.1.4 Microstructures after aging treatment

Microstructures of Samples 6 and 12 are shown in Fig. 6. In Sample 6, the α_S homogeneously precipitates from the β matrix between α_p and the PFZ in which no α_P is distributed after aging treatment. The α_p and α_{GB} have no observable change during the aging at 630 °C for 8 h (Fig. 6(a)). Meanwhile, in Sample 12 a mixture of α_P and α_S nearby the discontinuous α_{GB} is obtained (Fig. 6(b)).

After being annealing−solution−aging treated, α phase (α_p) in the as-deposited alloy grows up evidently. Compared with the microstructure in Fig. 1(b), the average width of α_{GB} in the as-deposited alloy increases from about 0.7 to 2.3 and 1.5 μm in Samples 6 and 12, respectively. And the average width of α_P increases from

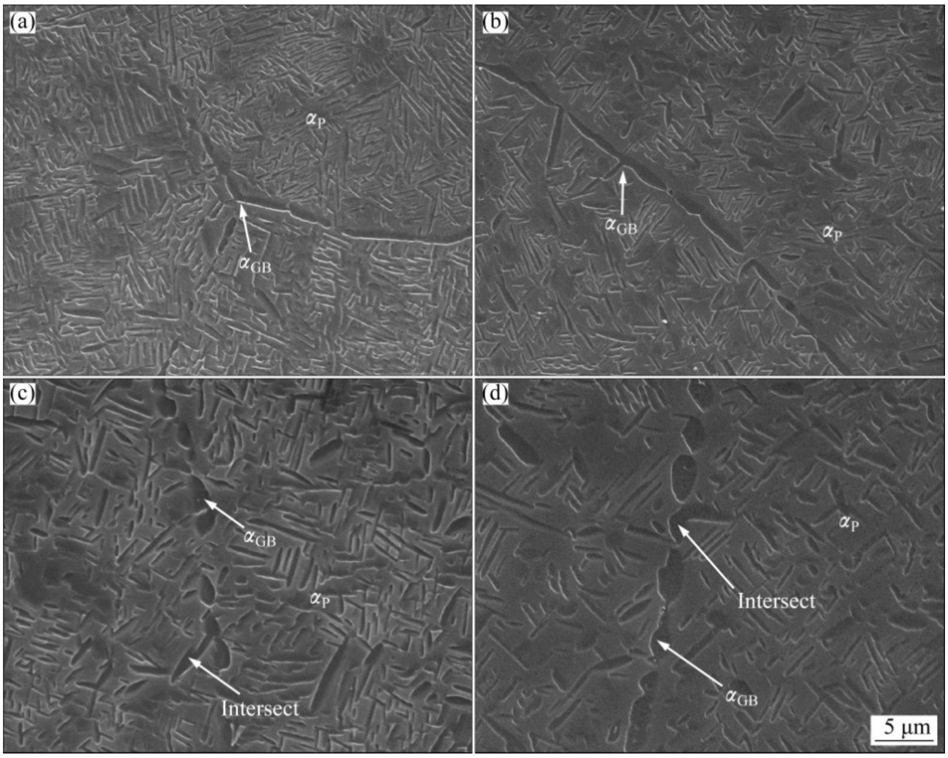

Fig. 5 Microstructures of Samples 8−11 treated at 800 °C for different solution time after 910 °C pre-annealing: (a) Sample 8, 0.5 h; (b) Sample 9, 1 h; (c) Sample 10, 2 h; (d) Sample 11, 4 h

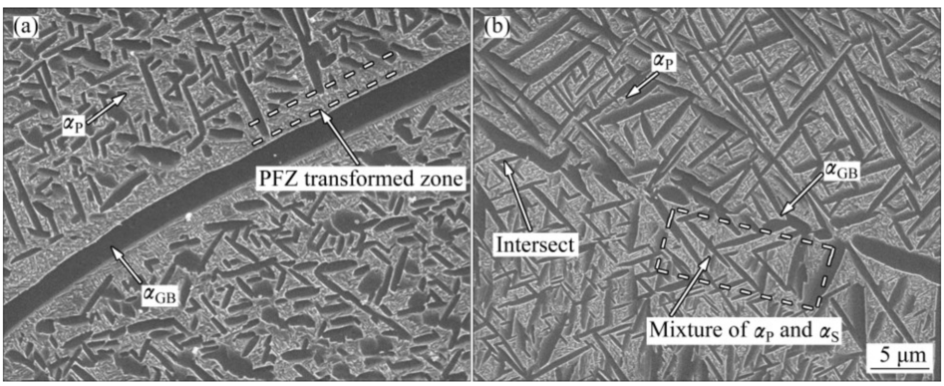

Fig. 6 Microstructures of samples after aging treatment: (a) Sample 6; (b) Sample 12

about 0.5 up to 1.4 and 0.7 μm as well after heat treatment, as shown in Fig. 7.

Different annealing temperatures in $\alpha+\beta$ or β phase region could affect the morphology of α_{GB} and the distribution of α_p near α_{GB}. However, the β grain morphology has not been changed. Large columnar grains still exist in the overlap zone of melting pool and small equiaxed grains and small column grains hardly grow up in the center zone during the heat treatment.

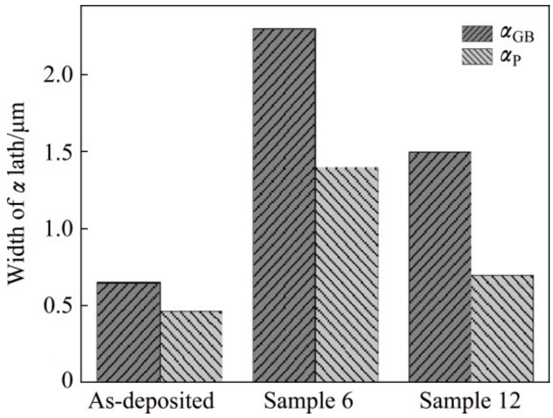

Fig. 7 Width of α lath in as-deposited alloy, Samples 6 and 12

3.2 Mechanical properties

3.2.1 Mechanical properties

Table 2 shows the tensile properties of the as-deposited and two different heat-treated LAM TC17 Samples 6 and 12. In comparison with the aviation standard (Q/S10−0345−2002) of TC17 titanium alloy, the as-deposited LAM TC17 sample exhibits the characteristics of higher strength but lower ductility, which result from the rapid solidification process and dispersion strengthening effect of ultra-fine α lath (Fig. 1(b)). The extreme low ductility is possibly due to the large prior β grains, the continuous α_{GB} and the high solid solubility resulting from the rapid cooling rate.

After the $\alpha+\beta$ annealing treatment (Sample 6), the ultimate tensile strength (UTS) and yield strength (YS) reduce by about 63 and 71 MPa, which are still sufficient to meet the aviation standard. It is worthwhile to note that the elongation (EL) and the area reduction (RA) at failure are 11.4% and 16.4, respectively, which increase by almost 119% and 40% compared with the as-deposited alloy. After the $\alpha+\beta$ annealing treatment, the tensile mechanical properties increase up to meet the aviation standard for the TC17 alloy. As for the β annealing treatment (Sample 12), both the strength and the ductility are higher than the aviation standard. The above results indicate that the annealing treatment either in the $\alpha+\beta$ region or in single β region is effective for the LAM TC17 titanium alloys to improve the mechanical properties.

Table 2 Room temperature tensile properties of different LAM TC17 samples

Sample	UTS/ MPa	YS/ MPa	EL/ %	RA/ %
As-deposited	1201±8	1164±17	5.2±0.7	11.7±1.5
Sample 6	1138±13	1093±11	11.4±1.0	16.4±3.5
Sample 12	1146±10	1104±13	8.8±0.3	18.0±2.5
Aviation standard (Q/S10−0345−2002)	≥1120	≥1030	≥7.0	≥15.0

3.2.2 Fractography

The tensile fractographs of as-deposited LAM TC17 sample are shown in Fig. 8. The specimen exhibits a mixture of intergranular and transgranular fractures due to the heterogeneity of the prior β grains. Shear lips surround the peripheral fracture. Several facets standing for different grains distribute on the intergranular fracture while transgranular fracture is smooth. A great quantity of tiny and shallow dimples form on the intergranular and transgranular fractures, indicating low ductility. Intergranular propagating secondary cracks exist in the equiaxed grains zone. Figure 9 shows the sub-surface morphology of the as-deposited TC17 tensile specimen. The coarse intergranular fracture area could be matched with the equiaxed grains zone and the smooth transgranular fracture area corresponds with the huge columnar grains zone. It can be inferred that the prior β grain morphology performs a great influence on the fracture mode of the as-deposited sample.

Tensile fracture surfaces of the two heat-treated LAM TC17 samples are shown in Fig. 10. Sample 6 is characterized by obvious demarcation between

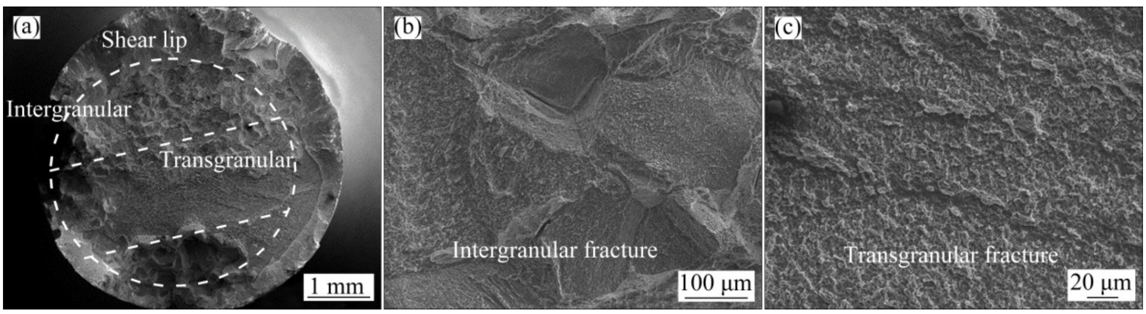

Fig. 8 Fractographs of as-deposited LAM TC17 tensile specimen: (a) Overview; (b, c) High magnification images

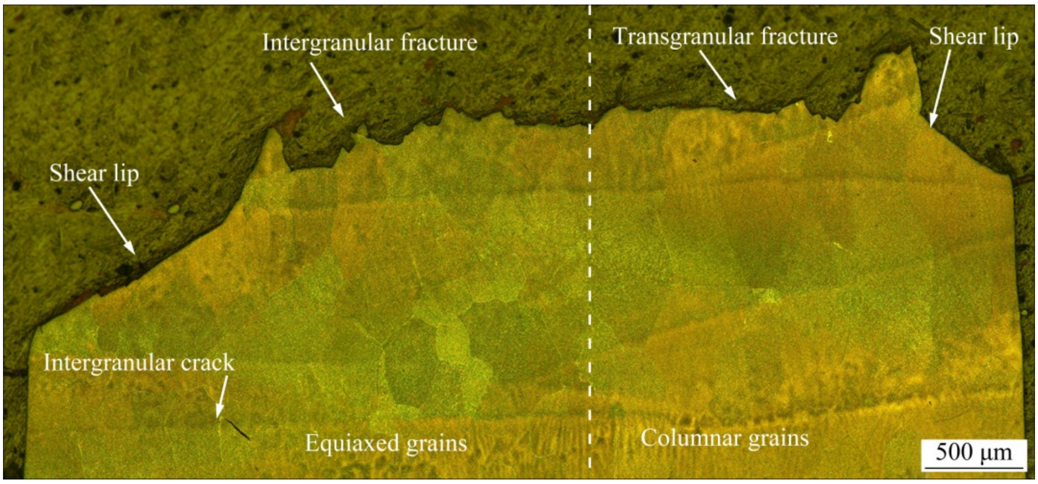

Fig. 9 Sub-surface morphology of as-deposited LAM TC17 tensile specimen

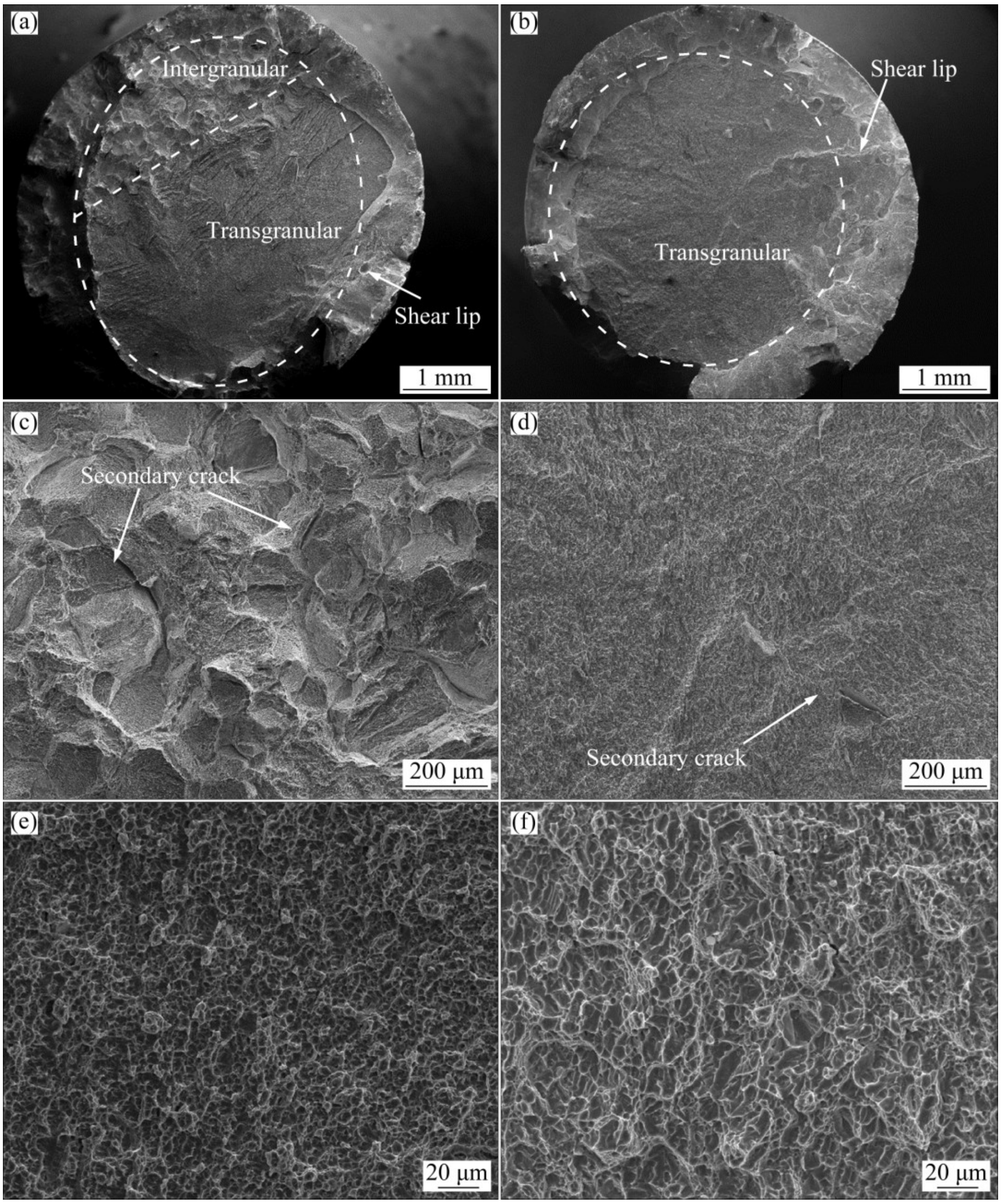

Fig. 10 Fractographs of heat-treated LAM TC17 tensile specimens: (a−c) Sample 6; (d−f) Sample 12

intergranular and transgranular fracture, which correspond to the equiaxed grains zone and the huge columnar grains zone, respectively (Figs. 10(a)−(c)). As for Sample 12, the fracture surface can be considered as transgranular fracture entirely (Figs. 10(d)−(f)).

Both of their sub-surface morphologies are shown in Fig. 11. It can be seen that the prior β grain morphologies of Samples 6 and 12 are similar to that of as-deposited alloy, which further indicates that the heat treatment has no effect on the prior β grains. The intergranular fracture area in Sample 6 (Fig. 11(a)) matches with the equiaxed grains and the transgranular fracture area matches with the overlap zone. Figure 11(b) reflects a smooth fracture surface of Sample 12 in which the transgranular crack propagation occurs not only in the huge columnar grains zone but also in the equiaxed grains zone. Cracks in Sample 6 tend to propagate along the continuous α_{GB} or the PFZ (Fig. 11(c)), resulting in the intergranular fracture. While in Sample 12, due to the breaking of the continuous α_{GB} and the eliminating of the PFZ, the crack grows across the discontinuous α_{GB} and intragranular α phase and β matrix randomly, leading to the transgranular fracture (Fig. 12).

In summary, the as-deposited sample exhibits excellent strength but lower ductility in tensile testing. After heat treatment, the mechanical properties have been improved obviously. Both strength and ductility have exceeded the aviation standard. The β annealing sample (Sample 12) possesses slight higher strength and equated ductility than the $\alpha+\beta$ annealing sample (Sample 6). Moreover, heat treatment could also change the fracture mechanism. The fracture mode of as-deposited alloy and Sample 6 is intergranular/ transgranular mixed fracture, while Sample 12 is typical transgranular fracture.

The improvements of mechanical performance as well as the transition of tensile fracture mechanism could be attributed to the microstructural evolution induced by heat treatments. The equiaxed grains, continuous α_{GB} and PFZ might cause intergranular fracture, and column grain

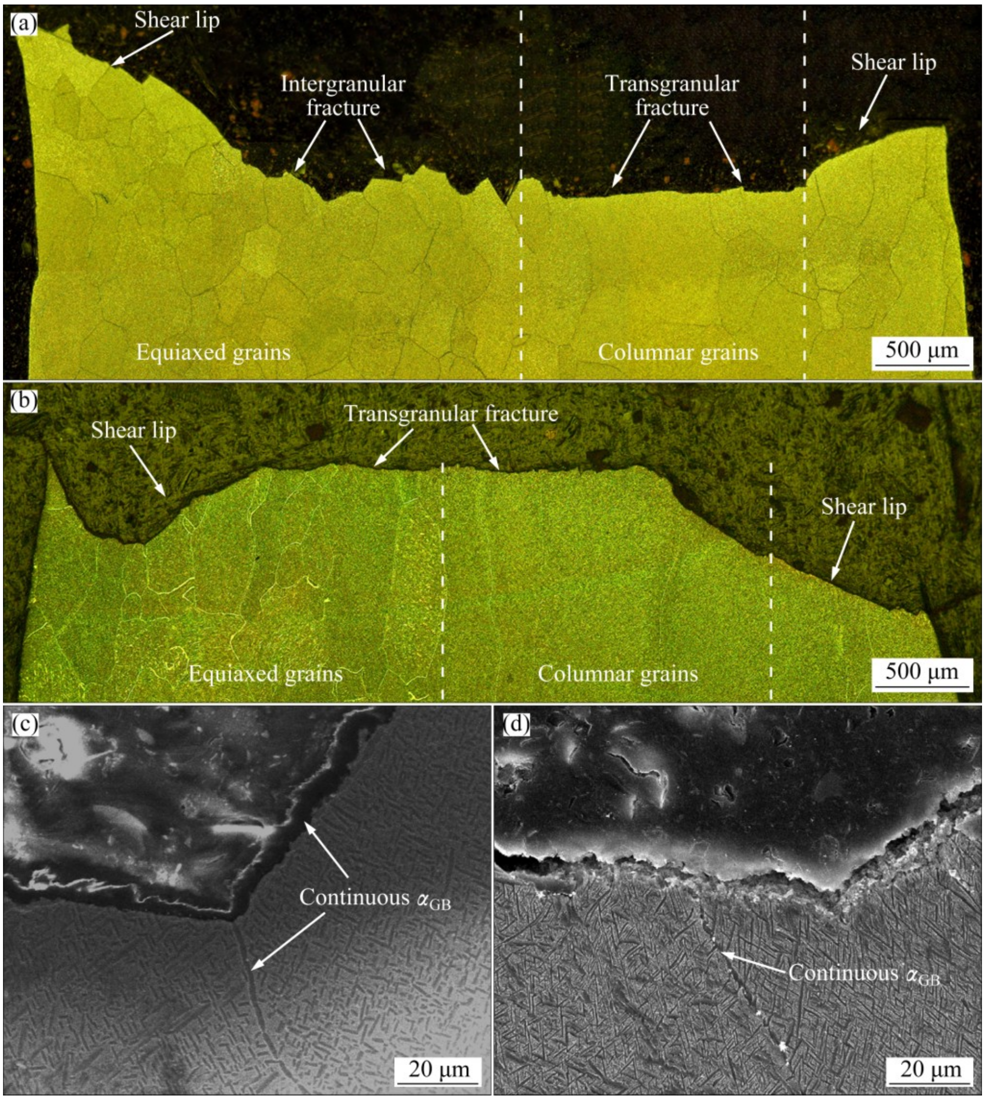

Fig. 11 Sub-surface morphologies of heat-treated LAM TC17 tensile specimens: (a, c) Sample 6; (b, d) Sample 12

along with discontinuous α_{GB} might cause transgranular fracture. Besides, the dimension of α lath might affect the mechanical properties, as wider α laths probably brought about lower strength in tensile test.

4 Discussion

Annealing in $\alpha+\beta$ and β phase region could influence the microstructure evolution in subsequent solution and aging treatment. Figure 13(a) illustrates the microstructure evolution of Sample 6 which was pre-annealed at 840 °C and solution and aging treated. The evolution process includes a reduction of α volume fraction (reduced from about 70% to 45%) and reduction of interfacial energy of α/β surface. During the α-to-β transformation, fine α phase near the large continuous α_{GB} would be dissolved more easily because it possesses higher surface area-to-volume ratio, namely higher interfacial energy, than the continuous α_{GB}. And α-stabilizer such as aluminum (Al) would be absorbed into α_{GB} phase and β-stabilizer such as molybdenum (Mo) and chromium (Cr) would be rich in the PFZ. This process results in the formation of the PFZ along the grain boundary [12,16,23].

In solution treatment, a small quantity of α phases precipitate and the phase equilibrium achieves soon, while the α_{GB} and the PFZ do not change obviously. Furthermore, with the holding time prolonging, the growth of α_P could be explained by the Oswald ripening theory. Smaller α_P owns higher curvature and energy, therefore, it would easily re-dissolve into β matrix. Similarly, larger α_P is more stable due to its lower curvature and energy, and continues to grow up gradually. In the final aging treatment, α_S would precipitate from the supersaturated β matrix uniformly. The PFZ transforms into a zone which only consists of fine α_S. As the coarse continuous α_{GB} can provide longer slip length of dislocations, the strength of α_{GB} is lower than that of the fine α/β lamellar microstructure in the PFZ transformed zone. Therefore, the crack is more likely to form at the interface between the PFZ and the α_{GB} and propagates along the α_{GB} or the PFZ. Thus, Sample 6 would perform intergranular fracture mode in the equiaxed grains zone.

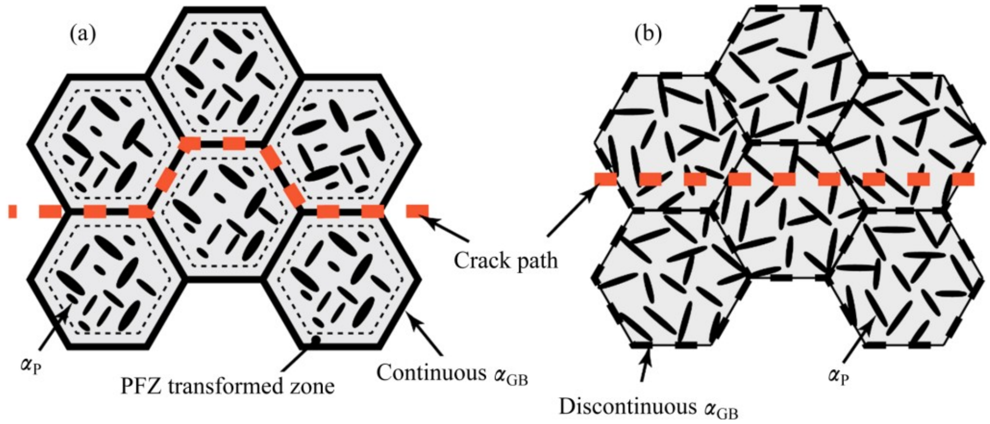

Fig. 12 Schematic illustration of crack growth path of two heat treatments: (a) Pre-annealed at 840 °C; (b) Pre-annealed at 910 °C

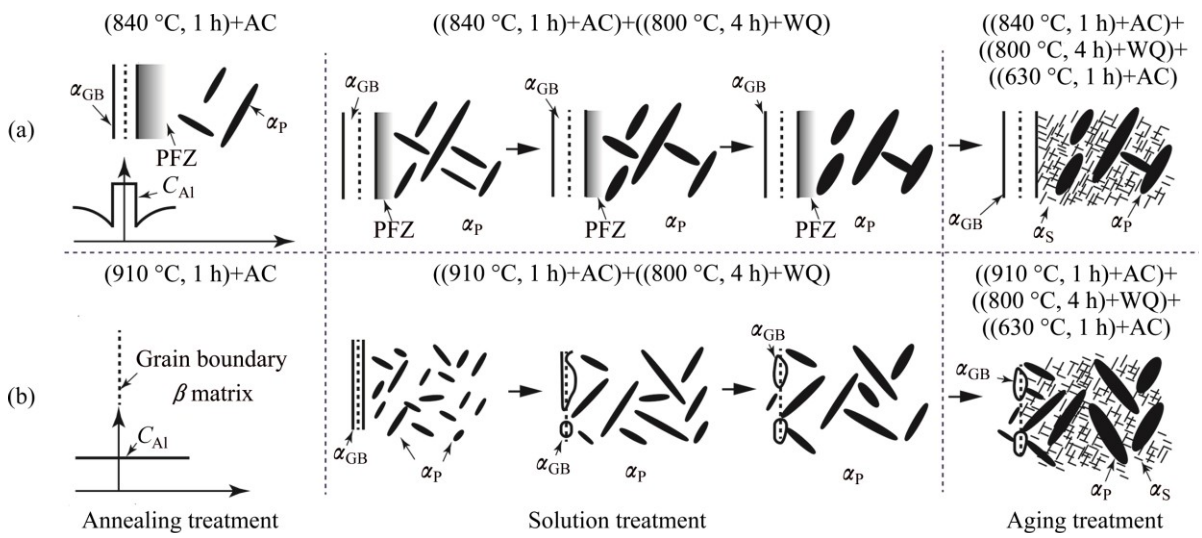

Fig. 13 Schematic illustration of microstructure evolution of two heat treatments: (a) Pre-annealed at 840 °C; (b) Pre-annealed at 910 °C

Likewise, Fig. 13(b) reveals the microstructure evolution of Sample 12 which was pre-annealed at 910 °C and solution and aging treated. As mentioned above, after annealing in β phase region, alloying elements distribute uniformly across the grain boundary and all the α phases dissolve into single β phase entirely. Therefore, during the solution treatment at 800 °C α phase could nucleate and grow at grain boundary and inward simultaneously, forming the α_{GB} and intragranular α_P, respectively. When the α_{GB} and α_P grow up, they would intersect with each other. Besides, the α_{GB} is discontinuous and α_p lath is not as thick as Sample 6 (Figs. 4 and 5). During aging treatment, α_S would precipitate in β matrix uniformly. A uniform mixture of α_S and α_P might be helpful to deflect the crack propagation from α_{GB} to grain inward. Therefore, Sample 12 performs typical transgranular fracture feature and a satisfactory ductility. Since the width of α_p lath is thinner than that in Sample 6, Sample 12 exhibits slightly higher strength.

Although the heat-treated LAM TC17 Samples 6 and 12 have performed relative acceptable mechanical properties as shown in Table 2, intergranular fracture is generally considered to be adverse to mechanical properties. However, heat treatments without deformation cannot refine the prior β grain morphology of LAM titanium alloys. Therefore, in order to further improve the mechanical properties, changing LAM processing parameters to gain uniform prior β grain morphology deserves to be explored in further studies.

5 Conclusions

1) The prior β grain morphology of laser additive manufacturing TC17 alloy consists of columnar and equiaxed grains. Huge columnar grains are parallel to the deposition direction, and small equiaxed grains and columnar grains are alternately placed. The microstructure exhibits ultra-fine basket-weave morphology with continuous α_{GB}. The mechanical properties of the as-deposited LAM TC17 show excellent strength and low ductility.

2) After annealing at 840 °C for 1 h, precipitate-free zone (PFZ) forms along the continuous α_{GB} and transforms into a zone filled with ultra-fine α_S but no α_P after solution and aging treatment. When annealing at 910 °C for 1 h, all α phases transform into β phase and the alloying elements distribute uniformly near the grain boundary. Discontinuous α_{GB} and uniform mixture of α_P and α_S near grain boundary form after subsequent solution and aging treatment.

3) The α+β annealed sample processes coarser α laths as well as slightly lower strength and equivalent ductility compared with that in β annealed sample. Both the heat-treated samples perform lower strength and better ductility than the as-deposited sample. The fracture modes of the as-deposited and the α+β annealed samples are intergranular/transgranular mixed fracture and mainly transgranular fracture, respectively.

References

[1] BANERJEE D, WILLIAMS J C. Perspectives on titanium science and technology [J]. Acta Materialia, 2013, 61: 844−879.

[2] BOYER R R. An overview on the use of titanium in the aerospace industry [J]. Materials Science and Engineering A, 1996, 213: 103−114.

[3] QIAN Ting-ting, LIU Dong, TIAN Xiang-jun, LIU Chang-meng, WANG Hua-meng. Microstructure of TA2/TA15 graded structural material by laser additive manufacturing process [J]. Transactions of Nonferrous Metals Society of China, 2014, 24: 2729−2736.

[4] TEIXEIRA J D C, APPOLAIRE B, AEBY-GAUTIER E, DENIS S, CAILLETAUD G, SPÄTH N. Transformation kinetics and microstructures of Ti17 titanium alloy during continuous cooling [J]. Materials Science and Engineering A, 2007, 448: 135−145.

[5] WANG T, GUO H, TAN L, YAO Z, ZHAO Y, LIU P. Beta grain growth behaviour of TG6 and Ti17 titanium alloys [J]. Materials Science and Engineering A, 2011, 528: 6375−6380.

[6] REN Hai-shui, TIAN Xiang-jun, LIU Dong, LIU Jian, WANG Hua-ming. Microstructural evolution and mechanical properties of laser melting deposited Ti−6.5Al−3.5Mo−1.5Zr−0.3Si titanium alloy [J]. Transactions of Nonferrous Metals Society of China, 2015, 25: 1856−1864.

[7] ZHANG Qiang, CHEN Jing, TAN Hua, LIN Xin, HUANG Wei-dong. Microstructure evolution and mechanical properties of laser additive manufactured Ti−5Al−2Sn−2Zr−4Mo−4Cr alloy [J]. Transactions of Nonferrous Metals Society of China, 2016, 26: 2058−2066.

[8] WANG H M, ZHANG S Q, WANG X M. Progress and challenges of laser direct manufacturing of large titanium structural components [J]. Chinese Journal of Lasers, 2009, 36: 3204−3209. (in Chinese)

[9] WU X, LIANG J, MEI J, MITCHELL C, GOODWIN P S, VOICE W. Microstructures of laser-deposited Ti−6Al−4V [J]. Materials & Design, 2004, 25: 137−144.

[10] BAUFELD B, BRANDL E, van der BIEST O. Wire based additive layer manufacturing: Comparison of microstructure and mechanical properties of Ti−6Al−4V components fabricated by laser-beam deposition and shaped metal deposition [J]. Journal of Materials Processing Technology, 2011, 211: 1146−1158.

[11] WEISS I, SEMIATIN S L. Thermomechanical processing of beta titanium alloys—An overview [J]. Materials Science and Engineering A, 1998, 243: 46−65.

[12] LUTJERING G, WILLIAMS J C. Titanium [M]. 2nd ed. Berlin: Springer, 2007: 203−258.

[13] SUN X, LIU D, TANG H, WANG H. Solid-state phase transformation and microstructure of laser direct manufactured TC17 titanium alloy components [J]. Rare Metal Materials and Engineering, 2013, 42: 724−729. (in Chinese)

[14] LIU C M, TIAN X J, TANG H B, WANG H M. Microstructural characterization of laser melting deposited Ti−5Al−5Mo−5V−1Cr−1Fe near β titanium alloy [J]. Journal of Alloys and Compounds, 2013, 572: 17−24.

[15] QIU C, RAVI G A, ATTALLAH M M. Microstructural control during direct laser deposition of a β-titanium alloy [J]. Materials & Design, 2015, 81: 21−30.

[16] LIU C M, WANG H M, TIAN X J, TANG H B, LIU D. Microstructure and tensile properties of laser melting deposited

Ti−5Al−5Mo−5V−1Cr−1Fe near β titanium alloy [J]. Materials Science and Engineering A, 2013, 586: 323−329.
[17] LU Y, TANG H B, FANG Y L, LIU D, WANG H M. Microstructure evolution of sub-critical annealed laser deposited Ti−6Al−4V alloy [J]. Materials & Design, 2012, 37: 56−63.
[18] TIAN X J, ZHANG S Q, LI A, WANG H M. Effect of annealing temperature on the notch impact toughness of a laser melting deposited titanium alloy Ti−4Al−1.5Mn [J]. Materials Science and Engineering A, 2010, 527: 1821−1827.
[19] THIJS L, VERHAEGHE F, CRAEGHS T, HUMBEECK J V, KRUTH J P. A study of the microstructural evolution during selective laser melting of Ti−6Al−4V [J]. Acta Materialia, 2010, 58: 3303−3312.
[20] MARTINA F, MEHNEN J, WILLIAMS S W, COLEGROVE P, WANG F. Investigation of the benefits of plasma deposition for the additive layer manufacture of Ti−6Al−4V [J]. Journal of Materials Processing Technology, 2012, 212: 1377−1386.
[21] AL-BERMANI S S, BLACKMORE M L, ZHANG W, TODD I. The origin of microstructural diversity, texture, and mechanical properties in electron beam melted Ti−6Al−4V [J]. Metallurgical and Materials Transactions A, 2010, 41: 3422−3434.
[22] ZHU Y, LIU D, TIAN X, TANG H, WANG H. Characterization of microstructure and mechanical properties of laser melting deposited Ti−6.5Al−3.5Mo−1.5Zr−0.3Si titanium alloy [J]. Materials & Design, 2014, 56: 445−453.
[23] LIU C M, WANG H M, TIAN X J, TANG H B. Subtransus triplex heat treatment of laser melting deposited Ti−5Al−5Mo−5V−1Cr−1Fe near β titanium alloy [J]. Materials Science and Engineering A, 2014, 590: 30−36.
[24] LEYENS C, PETERS M. Titanium and titanium alloys [M]. Darmstadt: Betz-druck GmbH, 2003: 37−57.
[25] LIU C M, WANG H M, TIAN X J, LIU D. Development of a pre-heat treatment for obtaining discontinuous grain boundary α in laser melting deposited Ti−5Al−5Mo−5V−1Cr−1Fe alloy [J]. Materials Science and Engineering A, 2014, 604: 176−182.
[26] ZHU Y, TIAN X, LI J, WANG H. The anisotropy of laser melting deposition additive manufacturing Ti−6.5Al−3.5Mo−1.5Zr−0.3Si titanium alloy [J]. Materials & Design, 2015, 67: 538−542.
[27] WANG T, ZHU Y Y, ZHANG S Q, TANG H B, WANG H M. Grain morphology evolution behavior of titanium alloy components during laser melting deposition additive manufacturing [J]. Journal of Alloys and Compounds, 2015, 632: 505−513.

热处理对激光增材制造 Ti−5Al−2Sn−2Zr−4Mo−4Cr 钛合金显微组织和力学性能的影响

朱言言，陈 博，汤海波，程 序，王华明，李 佳

北京航空航天大学 材料科学与工程学院 大型金属构件增材制造国家工程实验室，北京 100083

摘 要：研究热处理对激光增材制造 Ti−5Al−2Sn−2Zr−4Mo−4Cr 钛合金(TC17)的影响以优化其显微组织和力学性能。研究结果表明，激光增材制造 TC17 钛合金沉积态样品具有粗大的原始 β 柱状晶和等轴晶的混合晶粒形貌、晶内超细 α 片层和连续晶界 α 相(α_{GB})等典型特征。经 $\alpha+\beta$ 两相区 840 °C 预处理和标准固溶时效热处理后，连续晶界 α 相(α_{GB})粗化并且在其两侧形成不含初生 α 相(α_P)的晶界无析出区(PFZ)。经单相区 910 °C 预处理后，所有 α 相完全转变成 β 单相并且晶界附近溶质元素分布均匀，再经过标准固溶时效热处理形成明显断续的晶界 α 相(α_{GB})及呈均匀分布的晶内初生 α 相(α_P)和次生 α 相(α_S)。两种热处理工艺均可以明显提高激光增材制造 TC17 钛合金的综合力学性能，达到了 TC17 锻件航空标准规定值。

关键词：激光增材制造；TC17 钛合金；热处理；显微组织；力学性能

(Edited by Wei-ping CHEN)